



Maximum likelihood estimation for nanoindentation on sodium aluminosilicate hydrate gel of geopolymer under different silica modulus and curing conditions

Zhiyu Luo ^a, Wengui Li ^{a,*}, Yixiang Gan ^b, Kavya Mendu ^c, Surendra P. Shah ^c

^a School of Civil & Environmental Engineering, University of Technology Sydney, Sydney, NSW, 2007, Australia

^b School of Civil Engineering, The University of Sydney, Sydney, NSW, 2006, Australia

^c Department of Civil & Environmental Engineering, Northwestern University, Evanston, IL, 60208, USA

ARTICLE INFO

Keywords:

Alkali-activated fly ash geopolymer
Nanoindentation
Maximum likelihood estimation (MLE)
Nano/micromechanical properties
Sodium aluminosilicate hydrate (N-A-S-H)

ABSTRACT

As an important inorganic material, geopolymer has been widely used for ceramics and sustainable cement in concrete. Sodium aluminosilicate hydrate (N-A-S-H) gel known as the zeolite precursor gel has the most critical impact on the performance of geopolymer. The nano/micromechanical properties of N-A-S-H have been investigated in several studies, but the results are always inconsistent. A novel “compromise approach” using Maximum Likelihood Estimation (MLE) for deconvolution of nanoindentation data is introduced to fundamentally further understand this issue in this study. Correlation and difference of different statistical techniques are compared to clarify the rationality of this method. Multiple characterization techniques including microstructure observation at micro -and nano-scale, element analysis, and crystal identification are applied to reveal the mechanisms. The results indicate that the elastic modulus and hardness of the N-A-S-H gel in geopolymer under different silica modulus and curing conditions vary in a small range from 10.50 to 14.30 GPa and from 0.40 to 0.57 GPa, respectively. When applying statistical nanoindentation in geopolymer, two kinds of spurious phases, mixed phases and sub-phases are unavoidable. For the MLE method adopted, the errors generated from analytical technique were estimated to be only 0.68 and 0.13 GPa for elastic modulus and hardness, respectively.

1. Introduction

Fly ash is an industrial waste generated from coal-fired power plants. A considerable amount of fly ash has not been effectively treated every year, resulting in increasing concern about the consequent environmental pollution. Benefit from the alumina and silica rich nature, fly ash can be activated by alkali solution for varied applications. For instance, alkali activation of fly ash under heat curing or high temperature is applied for synthesizing sintered ceramic tiles [1], inorganic foams [2] and inorganic geopolymer cement [3–5]. Since the Portland cement industry contributes about 5–8% of manmade global carbon dioxide emissions [6], developing fly-ash based geopolymer cement is of great environmental significance [7–10].

Nanomechanical test techniques such as nanoindentation, modulus mapping, PeakForce quantitative nanomechanical mapping (PeakForce QNM), and nanoscratch are powerful tools for material analysis [11–15] and contribute a lot for the understanding of cement-based materials

[11,16–21]. As the most typical test technique, the nanoindentation technique has been widely used to test various properties of calcium silicate hydrate (C-S-H) gel in Portland cement paste including elastic modulus, hardness, creep, strength, fracture performance, etc [11, 22–26]. For the counterpart sodium aluminosilicate hydrate (N-A-S-H) gel in alkali-activated fly ash (AAFA), although there are nanoindentation studies for the investigation of elastic modulus, hardness and creep properties [27–31], the related studies are far less than that of C-S-H. The insufficient studies not only leave a gap in research but also lead to inconsistent results. Typically, based on the investigation on heat-cured AAFA, ambient cured AAFA and heat-cured alkali-activated metakaolin, Němeček et al. [27] found that the mature N-A-S-H gels (6 months) show almost the constant intrinsic Young's modulus of 17–18 GPa, which is independent of the precursor material and the temperature curing regime. However, the studies by others indicate that the elastic modulus of N-A-S-H gel is not a constant value. The elastic modulus of N-A-S-H gel is 16.3 GPa in the study by Das et al. [28],

* Corresponding author. School of Civil & Environmental Engineering, University of Technology Sydney, NSW, 2007, Australia.

E-mail address: wengui.li@uts.edu.au (W. Li).

4.44–16.78 GPa in the study by Lee et al. (after 28-day) [29] and 11–25 GPa in the study by Ma et al. (at 28 days) [30]. For the counterpart C-S-H gel in Portland cement paste, lots of studies indicate that the elastic modulus of it is an intrinsic material invariance property, in which, some of them are tested at 28 days [32] and also some found that the elastic modulus at 28 days is similar to results at the longer time of curing of 0.5 year or 1 year [33].

For the nanomechanical studies of AAFA mentioned above, the least-square estimation (LSE) method is normally adopted to fit the frequency density histogram and obtain nano/micromechanical properties of each phase correspondingly in the deconvolution process. One thing to note is different bin sizes such as 2 GPa [30] and 1 GPa [27,28] and different phase number of 3 [30] or 4 [27,29] were chosen in different studies. It has been realized that the deconvolution results would depend on the bin size used when adopting the LSE method [34]. The number of phases set should also be an important factor. It is questionable that if the normally used phase number of 4 in the deconvolution of Portland cement paste is still feasible to generate a pure gel phase in the deconvolution of AAFA. Therefore, the correct understanding of the elastic modulus of N-A-S-H should be based on a premise that the test and data deconvolution analysis method should be consistent and reliable to eliminate errors of the result caused by deconvolution method itself.

Maximum likelihood estimation (MLE) is another technique used for the deconvolution of nanoindentation data. This technique has the benefit of independent on bin size but is rare to be used. These limited studies typically include the research for Portland cement paste [35,36], calcium sulfoaluminate cement paste [37], and magnesium oxychloride cement paste [38]. However, there is no detailed introduction for this method, and the gel phase obtained by MLE is found to be a mixture of gel and crystals in research of [36]. Coupling of Energy Dispersive X-Ray Spectroscopy (EDS) with statistical nanoindentation is a strategy to identify and then obtain the properties of the gel phase [35,39]. However, the properties of gel would be accurate only when sufficient test data is collected for it (average value), which leads to very time-consuming element analysis on points. Errors are easy to be accumulated in the manual matching of the EDS detector with faint nanoindentation marks. In addition, the involved volume of EDS and nanoindentation is matched based on the gel phase, which may not match on mixed phases. Importantly, the element ratio of N-A-S-H is in a variable range [40]. It is impossible to identify if there are crystals such as mullite and quartz in N-A-S-H by element analysis. In this study, a two-dimensional Gaussian mixture model (GMM) including both elastic modulus and hardness information was used to describe the micro-mechanical distribution of AAFA with different silica modulus and under different curing conditions. Then, a “compromise approach” using MLE was proposed for deconvolution to investigate the nano-/micromechanical properties of N-A-S-H gel. Error estimation, comparative analysis of different deconvolution techniques and microstructure characterizations were conducted to provide more sights for the understanding of the results obtained and the deconvolution technique adopted.

2. Experimental program

2.1. Sample preparation

Low calcium fly ash was used as the raw material with chemical composition given in Table 1. Alkali solution is sodium hydroxide or sodium silicate with different silica modulus of 1 or 1.5. Sodium hydroxide solution was prepared by dissolving sodium hydroxide pellets

into water. The sodium silicate was purchased from PQ Corporation with an original modulus of 2.07 (14.7% of Na₂O and 29.4% of SiO₂). Cooled sodium hydroxide solution was incorporated into sodium silicate solution to adjust the silica modulus of the solution to the designed value of 1 or 1.5. The mixture ratios for samples are shown in Table 2, where the same water to solid ratio is applied to keep the water content in the bind of each sample similar. Fly ash and alkali solution were mixed by Hobart mixer for 5 min and cast into 50 mm × 50 mm × 50 mm cubic plastic mould. The fresh paste was vibrated for 3 min on a vibration table and then sealed by plastic film. For heat cured samples, they were put into an oven with heat treatment of 70 °C for 24 hr. After that, samples were removed from the oven and put into a standard curing cabinet (temperature of 22 °C, relative humidity of 95%) for further curing. The standard cured sample was always stored in the standard curing cabinet once finished casting and vibration of the sample.

Microstructure observation was conducted on small pieces of crushed samples while BSE imaging and nanoindentation test were operated on polished samples. Cutting machine was used to take out the core part of the cubic samples, which was then cast in epoxy resin and subjected to grind and polish. Abrasive papers with grits of 320, 600 and 1200 were used to grind the samples with each grade lasted for 10 min. 0.3 μm alumina and 0.05 μm cerium oxide slurry were used for further polishing samples with each grade lasted for 40 min. Residual particles present on the surface of samples after each polish procedure were removed by ultrasonic cleaning of samples in isopropanol for 3 min. After finishing the sample preparation, samples were dried by vacuum oven under 50 °C for 72 hr, and then stored in a vacuum desiccator.

2.2. SEM and XRD characterization

Zeiss EVO SEM equipped with an EDS detector was used for the microstructure observation and element analysis of AAFA samples under the voltage of 15 kV [41,42]. Bruker D8 Discover diffractometer was adopted to detect crystals in raw material fly ash and reacted AAFA samples.

2.3. Statistical nanoindentation

Nano/micromechanical properties of samples were tested by Agilent G200 Nano Indenter after 28 days of curing. Nine 10 × 10 grid nanoindentations were conducted for each sample with a grid spacing of 15 μm. For an individual nanoindentation test procedure, Berkovich tip is pressed into the sample with a constant speed of 0.2 mN/s until it

Table 2
Mixture design and curing condition of geopolymers.

Samples	SiO ₂ /Na ₂ O (silica modulus)	Na ₂ O/fly ash	w/s	Curing condition
AAFA-M1-S	1	8%	0.338	Standard curing
AAFA-M0-H	0 (NaOH)	8%	0.338	Heat curing at 70 °C for 24 h
AAFA-M1-H	1	8%	0.338	Heat curing at 70 °C for 24 h
AAFA-M1.5-H	1.5	8%	0.338	Heat curing at 70 °C for 24 h

Note: w/s is water to solid ratio. ‘M0’, ‘M1’ or ‘M1.5’ behind AAFA means the silica modulus of alkali solution to make AAFA is 0, 1 or 1.5. ‘H’ or ‘S’ behind AAFA denotes the corresponding curing condition is heat curing or always standard curing.

Table 1
Chemical composition of fly ash.

Oxide	Al ₂ O ₃	CaO	SiO ₂	Fe ₂ O ₃	K ₂ O	MgO	Na ₂ O	MnO	P ₂ O ₅	TiO ₂	LOI
Weight (%)	25.21	1.73	64.55	2.85	1.47	0.41	0.48	0.07	0.19	0.91	1.54

reaches the predetermined maximum force of 2 mN. The maximum force is sustained for 5 s and then it is unloaded to 10% of the maximum force with a speed of 0.18 mN/s. Based on this loading procedure, the average penetration depth in nanoindentation tests is normally slightly more than 200 nm, which is thought to be a suitable depth to satisfy scale separability condition, avoid multiple phase response as shown in Eq. (1), and also avoid interference from surface roughness [43,44].

$$d \ll h_{\max} < D/10 \quad (1)$$

where d is the largest heterogeneity of geopolymers phases which is reported to be about 5 nm [40], D is the characteristic size of microstructure, more than about 4 μm can be found even just 7% Na₂O (Ms = 1) is used [45].

The reduced modulus and hardness of materials are determined by Eqs. (2) and (3). According to the load-depth curves, the abnormal nanoindentation test points that violate the self-similarity of continuum nanoindentation analysis were removed before analysis.

$$H = \frac{P_{\max}}{A} \quad (2)$$

$$S = \frac{dP}{dh} |_{h=h_{\max}} = \frac{2}{\sqrt{\pi}} E_r \sqrt{A} \quad (3)$$

where P and h are the indentation load and indentation depth, respectively; The S is the initial unloading stiffness; E_r is the reduced elastic modulus, which contains the elastic response of both indenter tip and tested material; A is the projected contact area at the maximum depth.

The elastic modulus of the tested sample can be calculated based on the relation between elastic modulus and reduced modulus as given in Eq. (4). The elastic modulus was combined with hardness for deconvolution.

$$\frac{1}{E_r} = \frac{1 - \nu^2}{E} + \frac{1 - \nu_i^2}{E_i} \quad (4)$$

E_i and ν_i are the elastic modulus and Poisson's ratio of the indenter, respectively; E and ν are the corresponding parameters for sample.

2.4. Deconvolution technique

The micromechanical distribution of each phase is assumed to be a Gauss distribution as shown in Eq. (5). Two-dimensional Gauss is adopted to include both elastic modulus and hardness information, where $x = (M, H)^T$ is a column vector, which is considered to be more reasonable for further analysis than the model just reflects a single property. Gaussian mixture model (GMM) is used to describe the nano/micromechanical properties distribution of the multiple phases AAFA system as given in Eqs. (6) and (7).

$$\mathcal{N}(x|\mu, \Sigma) = \frac{1}{\sqrt{\det(2\pi\Sigma)}} \exp\left(-\frac{1}{2}(x-\mu)^T \Sigma^{-1} (x-\mu)\right) \quad (5)$$

$$p(x) = \sum_{k=1}^K \pi_k \mathcal{N}(x|\mu_k, \Sigma_k) \quad (6)$$

$$\sum_{k=1}^K \pi_k = 1 \quad (7)$$

where π_k , μ_k and Σ_k are the corresponding weighting coefficient, mean value and covariance of the k th component, respectively.

The parameters of the GMM are estimated by the Maximum Likelihood Estimation (MLE) method, with the log-likelihood function given by Eq. (8). Expectation-Maximization (EM) algorithm [46] with the E step given by Eq. (9) and M step given by Eqs. (10)–(12) was used to find the mean value, covariance and weighting coefficient of each

component that make the log-likelihood function achieves the maximum value and then obtain the nano/micromechanical properties of each phase. K-means algorithm was combined used to find suitable initial values for parameters to reduce the time needed for iteration calculation. At least 1000 times of repeated calculation with random initial input values were made to find the global optimum value.

$$\ln L = \sum_{n=1}^N \ln \left\{ \sum_{k=1}^K \pi_k \mathcal{N}(x_n|\mu_k, \Sigma_k) \right\} \quad (8)$$

$$\gamma(z_{nk}) = \frac{\pi_k \mathcal{N}(x_n|\mu_k, \Sigma_k)}{\sum_{j=1}^K \pi_j \mathcal{N}(x_n|\mu_j, \Sigma_j)} \quad (9)$$

$$\mu_k = \frac{1}{N_k} \sum_{n=1}^N \gamma(z_{nk}) x_n \quad (10)$$

$$\sum_k = \frac{1}{N_k} \sum_{n=1}^N \gamma(z_{nk}) (x_n - \mu_k) (x_n - \mu_k)^T \quad (11)$$

$$\pi_k = \frac{N_k}{N} \quad (12)$$

$$N_k = \sum_{n=1}^N \gamma(z_{nk}) \quad (13)$$

where $\gamma(z_{nk})$ is the posterior probability. π_k , μ_k and Σ_k are the weighting coefficient, mean value and covariance of the k th component, respectively. N is the total number of observed data, corresponding to nanoindentation testing data here.

Bayesian Information Criterion (BIC) shown in Eq. (14) was adopted [46,47] to penalize the overfitting errors of the GMM to help find the suitable number of components to describe the nano/micromechanical properties distribution of AAFA. After calculation, the raw nanoindentation test data are clustered to the corresponding component according to the maximum posterior probability where achieved 95%, 80% and 70% confidence ellipses for each estimated component model are plotted correspondingly.

$$\text{BIC} = k \ln n - 2 \ln L \quad (14)$$

3. Characterization of AAFA

The typical microstructure of AAFA is presented in Fig. 1, which mainly consists of unreacted fly ash, partially reacted fly ash, matrix (N-A-S-H) surrounding fly ash particles, crystals, and defects (pores, microcracks). From the appearance of the partially reacted particles A and B in Fig. 1(b), it is easy to realize that there are different kinds of fly ash particles in raw materials. Microscale crystals can be clearly found in Fig. 1(c). Besides, the SE image in Fig. 1(d) reveals that the appearance of the matrix is still very dense even under 8000 times of magnification. In fact, the microstructure observation of AAFA can't fully show the heterogeneous nature of AAFA. The uneven distribution of elements is shown in Fig. 2 to provide a further understanding of this issue. Diverse fly ash with different chemical compositions can be found in the second figure, which is one of the main reasons for the highly heterogeneous characteristics of AAFA. Typically, the brightest fly ash particle is rich in Fe, while other particles are normally rich in Al and Si. Even if a dense matrix is observed by SE, it may still have different chemical compositions and varied nano/micromechanical properties in different locations due to the mix of N-A-S-H with other phases (e.g. crystals and tiny unreacted particles).

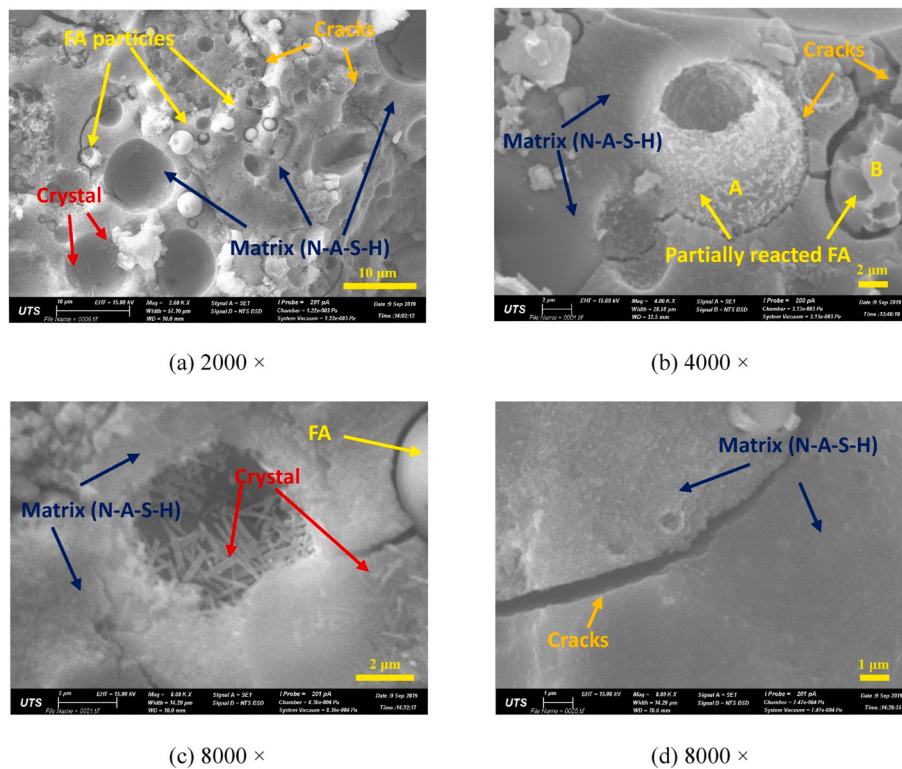


Fig. 1. Microstructure of alkali-activated fly ash geopolymers.

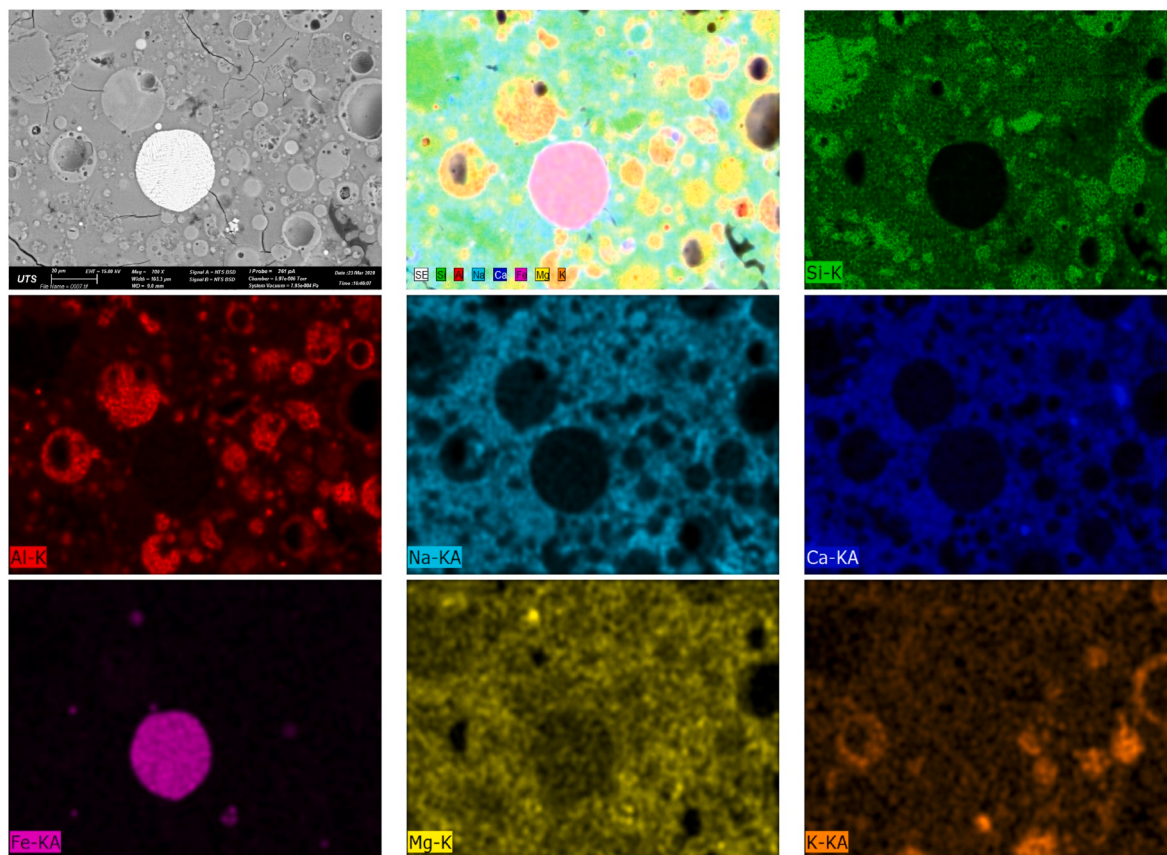


Fig. 2. EDS element maps of alkali-activated fly ash geopolymers.

4. Deconvolution analysis and results

4.1. Compromise approach for the mismatch between real components and micromechanical peaks

Normally, the number of phases set for the deconvolution of statistical nanoindentation data is the real number of components in the sample [34,48]. However, this kind of match is not always reasonable. For this study, different kinds of fly ash particles composed of different elements would have different nano/micromechanical properties. The micromechanical distribution of fly ash may vary in a large range and overlap other phases such as crystal and mixed phase. The involved range of gel is known as 3–4 times of the nanoindentation depth [49]. Crystals and unreacted particles at the submicron and nano-scale would be mixed with N-A-S-H gel to be identified as mixed phases. For crystal and unreacted particles at a larger scale, the interaction of the different phases (e.g. gel and unreacted FA) at the region around interface would also lead to the identification of mixed phases. Another factor that cannot be ignored is the limited test number in any real test, which would be not able to fully present the real information of micromechanical distribution. Because of very few data acquired, some real phases with a very small proportion may be mixed into other phases instead of identifying as an individual peak in the deconvolution process. In the meantime, due to discrete data, some phases with large proportion and broad distribution are possibly breakdown into several sub-phases in deconvolution. Both the mixed phases and sub-phases are spurious phases and can appear simultaneously. When increasing the number of components for deconvolution, the difference is the sub-phases would increase while the mixed phases would decrease.

Both the nature of the sample, the test factors and the deconvolution parameters (number of components for MLE) would be responsible for the generation of mixed phases and sub-phases. It is virtually impossible to reconcile these two kinds of spurious phases to obtain the accurate nano/micromechanical properties of each real component in geopolymer by statistical nanoindentation. The strategy of this study is using a “compromise approach”, focusing on the most crucial phase N-A-S-H gel merely. The nano/micromechanical properties of some phases like crystals are not able to be obtained by statistical nanoindentation since there are intrinsic limitations from the size and proportion of the phase (nature of the sample), and the involved volume (test factors) as well. However, as a gel phase, N-A-S-H has a large proportion, suitable characterization size. In addition, the nano/micromechanical properties (elastic modulus and hardness) of it would be significantly smaller than the unreacted fly ash particles, crystal, and significant mixed phases. Those factors ensure that the micromechanical peak of the N-A-S-H gel

can be separated from mixed phases by increasing the number of components in the deconvolution. In this process, the individual phase N-A-S-H is sometimes obtained by sacrificing the accuracy of other phases as spurious phases (sub-phases) may be introduced.

4.2. Deconvolution results for AAFA-M1-S

For AAFA cured under standard curing condition, the deconvolution results of the phase ($k \leq 9$) or the two phases ($k > 9$) which show the minimum nano/micromechanical properties are listed in Table 3. Some key deconvolution results are revealed in Fig. 3. These results indicate that when k (the number of phases) is 2 or 3 or 4, the corresponding phase has high variance values. For instance, for the model with 4 components, the elastic modulus of the “blue phase” ranges from very small values to almost 50 GPa, while the hardness of it ranges from around 0 GPa to more than 2 GPa. Besides, high average elastic modulus and hardness values are observed. When the number of components reaches 5, a new phase, phase 2 in Fig. 3(d) with small nano/micromechanical properties and variances is separated from the phase 1 in the model with 4 components. For this new phase, the elastic modulus and hardness standard deviation of it are 3.61 and 0.25, respectively, which are similar to the value reported for the C-S-H gel in cement pastes [22]. In addition, the elastic modulus of 11.20 GPa and hardness of 0.41 GPa of this phase are also close to lots of results reported for low-density C-S-H [22], although a bit low. Therefore, the big phase, phase 1, in the model with 4 components should be a phase mixed by gel and other inclusions, while the phase 2 separated from it in the model with 5 components should be the gel phase. The reinforcing effect of the inclusions enhances the nano/micromechanical properties of the mixed phase. The presence of multiple phases induces a large range of variation for both elastic modulus and hardness.

As revealed in Table 3, there is a slight decrease in the elastic modulus and hardness of the gel phase when the number of components in the model increases from 5 to 9. A more significant change occurs when the number of components reaches 10, where the phase 3 in the model with 9 components is decomposed into two small phases, phase A and phase B shown in Fig. 3 (h). The properties of the phase A and phase B remain stable even the number of components increases to 12. Increasing the number of components further makes the calculation difficult to converge with lots of random initial input values and hard to find the real global optimal solution. Therefore, the calculation is stopped after the model reaches 12 components even if it does not reach the optimal Bayesian value (minimum value).

Table 3
Deconvolution result for AAFA-M1-S (clustered blue points and red points).

k	M [GPa]	H [GPa]	f	BIC	C		
					C11	C12 = C21	C22
2	32.96	2.95	65.30%	16050.70	296.21	32.10	5.26
3	22.32	1.13	29.73%	15568.81	116.77	5.87	0.42
4	23.56	1.18	30.09%	15466.12	126.07	6.66	0.48
5	11.20	0.41	7.27%	15403.81	13.03	0.62	0.06
6	11.18	0.41	7.28%	15363.51	13.01	0.61	0.06
7	10.76	0.36	7.16%	15326.70	11.85	0.49	0.05
8	10.76	0.36	7.16%	15298.94	11.87	0.49	0.05
9	10.76	0.36	7.23%	15278.04	11.92	0.49	0.05
10-phase A	11.08	0.45	5.15%	15255.38	14.24	0.62	0.04
10-phase B	9.87	0.13	1.86%	15255.38	5.66	0.12	0.003
11-phase A	11.37	0.46	5.57%	15243.42	14.93	0.66	0.04
11-phase B	9.89	0.13	1.86%	15243.42	5.70	0.12	0.003
12-phase A	11.10	0.45	5.10%	15233.15	14.19	0.63	0.04
12-phase B	9.86	0.13	1.86%	15233.15	5.63	0.12	0.003
Ave_5-7	11.05	0.40	7.24%	–	12.63	0.57	0.06

Note: k is the number of phases. The numbers in the column of “M” and “H” refer to mean value of elastic modulus and hardness, respectively. f is the proportion of the phase. C is covariance matrix, where C11 is the variance of elastic modulus, C22 is the variance of hardness and C12 is the covariance of modulus and hardness.

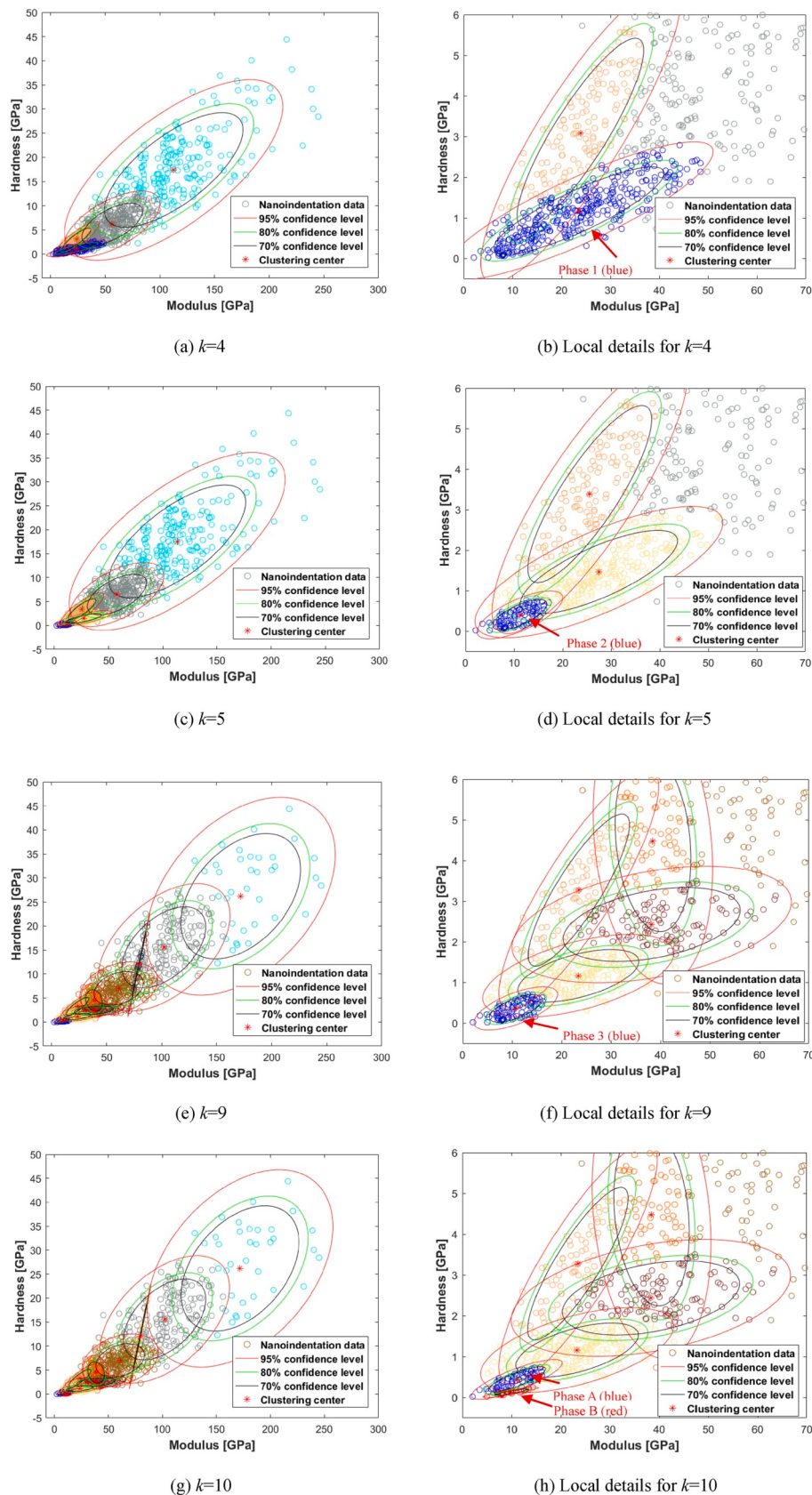


Fig. 3. Deconvolution of nanoindentation data (elastic modulus and hardness) for AAFA-M1-S.

4.3. Deconvolution results for AAFA-M0-H

Table 4 and **Fig. 4** present the deconvolution results for the NaOH activated fly ash sample. For this sample, a phase with nano/micro-mechanical properties conforming to the empirical knowledge (LD C-S-H and N-A-S-H identified in AAFA-M1-S) of the gel phase presents when k is 3. Then, the properties of the phase decrease slightly with the increase in the number of components until 6 components are given to the model. For the models with 3–6 components, the properties of the phase listed in **Table 4** are similar to some results for standard cured sample AAFA-M1-S in **Table 3**. However, this phase is decomposed into two smaller phases when k is 7, which can be observed from **Fig. 4(b), (d) and (f)**. These two phases persist even if there are 12 components in the model as shown in **Table 4**.

4.4. Deconvolution results for AAFA-M1-H

For the AAFA-M1-H sample, the deconvolution results are revealed in **Fig. 5**. The results indicate that the properties of AAFA-M1-H start to vary in a small range when the number of components reaches 3, and the final stable phase is generated from the model with 8 components to the model with 12 components. However, even for the model with 12 components the variance of elastic modulus and hardness of this phase are still large values, which are 60.32 and 0.27, respectively. Besides, the elastic modulus, hardness, and proportion of the phase in the model

Table 4
Deconvolution results for AAFA-M0-H (clustered blue points and brown points).

k	M [GPa]	H [GPa]	f	BIC	C		
					C11	C12 = C21	C22
2	20.74	1.33	65.81%	10247.74	91.06	6.07	0.64
3	11.49	0.48	17.77%	10054.60	19.84	1.04	0.07
4	10.22	0.39	14.11%	9961.75	14.01	0.67	0.05
5	9.78	0.36	12.10%	9930.88	12.40	0.57	0.04
6	9.78	0.36	12.13%	9911.21	12.41	0.57	0.04
7-phase A	7.84	0.25	8.23%	9893.07	6.26	0.24	0.02
7-phase B	13.28	0.60	8.24%	9893.07	5.58	0.01	0.03
8-phase A	7.81	0.25	8.13%	9882.40	6.32	0.24	0.02
8-phase B	13.40	0.61	9.71%	9882.40	7.11	0.08	0.04
9-phase A	7.76	0.25	7.98%	9880.84	6.14	0.23	0.02
9-phase B	13.29	0.60	8.26%	9880.84	5.77	0.05	0.03
10-phase A	7.83	0.25	8.23%	9874.01	6.25	0.24	0.02
10-phase B	13.24	0.60	8.19%	9874.01	5.59	0.01	0.03
11-phase A	7.21	0.20	5.78%	9865.82	6.17	0.19	0.01
11-phase B	12.80	0.56	10.10%	9865.82	7.46	0.11	0.03
12-phase A	7.78	0.25	8.10%	9857.43	6.14	0.23	0.02
12-phase B	13.23	0.60	8.60%	9857.43	6.05	0.03	0.03
Ave_3-5	10.50	0.41	14.66%	–	15.42	0.76	0.05

Note: k is the number of phases. The numbers in the column of “M” and “H” refer to mean value of elastic modulus and hardness, respectively. f is the proportion of the phase. $C11$ is the variance of elastic modulus, $C22$ is the variance of hardness and $C12$ is the covariance of modulus and hardness.

with 12 components are 22.69 GPa, 1.29 GPa, and 30.25%, respectively, which are similar to the mixed phase (blue phase, $k = 4$) in AAFA-M1-S. Therefore, the final stable phase in models with 8–12 components is not regarded as the possible N-A-S-H gel phase. The second deconvolution is conducted for the final stable phase, based on the clustered data of the phase (phase 1) in the model with 12 components as shown in **Fig. 6(b)**.

The results for the second deconvolution are listed in **Table 5** and **Fig. 6**. Firstly, one component (12-1) is set for deconvolution, which generates results very close to the estimated results for the final stable phase in the model with 12 components in the first deconvolution. It means that the clustered data is reliable to reflect the properties of the estimated final stable phase in the first deconvolution and can be used for the second deconvolution. For the second deconvolution, a stable phase, phase 2 shown in **Fig. 6(c)** and (d) is separated from phase 1 in the model with 3–7 components. The properties of it are in line with empirical knowledge for the gel phase. Further deconvolution with an increased number of components would lead to no more stable phase with reasonable proportion due to the limited data. Therefore, a maximum of 7 components is assigned to the model for deconvolution.

4.5. Deconvolution results for AAFA-M1.5-H

The deconvolution results for the AAFA-M1.5-H sample are shown in **Fig. 7** and **Table 6**. For this sample, the variation of the properties of phases starts in a small range when the number of components reaches 3. The more stable phase presents from the model with 5 components. Afterward, the properties of this phase do not change evidently even if the number of components reaches 12.

5. Analysis and discussion

5.1. Determination of gel phases in geopolymers

For the deconvolution results given above, one crucial step is to determine the gel phase correctly. Theoretically, the optimal Gaussian mixture model can be determined by the Bayesian Information Criterion (BIC). In this study, the BIC does not reach the optimum value, which means more components are needed. Although the number of test points in this study is even more than three times of some other studies, the data is still sparse at some locations, which would lead to peaks for sub-phases. The presence of phases with a very small proportion in models indicates that some points are misidentified as an individual phase. In fact, BIC evaluates the whole model. It is not necessary to achieve the optimal as this study focuses on the gel phase only. The empirical knowledge of the gel phase is used for determining the N-A-S-H gel.

As typically analyzed above for AAFA-M1-S, the phase in the model with 4 components and has high elastic modulus and hardness of 23.56 GPa and 1.18 GPa should be the mixed phase, while the phase in 5 components model with elastic modulus and hardness of 11.20 GPa and 0.41 GPa, respectively, is consistent with the features of gel phase. It is easy to find that there are similar mixed phase and gel phase in the other three kinds of samples. When further increasing the number of components, the nano/micromechanical properties and proportion of the gel phase in AAFA-M1-S and especially AAFA-M0-H are decreased. In the deconvolution process, few components for a model may make the phase that has minimum nano/micromechanical properties a mixed phase as mentioned. Actually, too many components may result in the excessive separation of the gel phase, breaking the single gel phase into sub-phases. The gel phase in 5–9 components models of AAFA-M1-S just has a small proportion of slightly more than 7.27%, the breakdown of the single phase into two phases with very small proportions (even 1.86%) should be more ascribed to the spurious phase generated when too much phase number assigned to the model. For the results slightly changed from the 5 components model to 9 components model, it is hard to ascertain if it is a refinement of the result by removing more inclusion or an excessive separation of the gel phase. In this study, if the possible

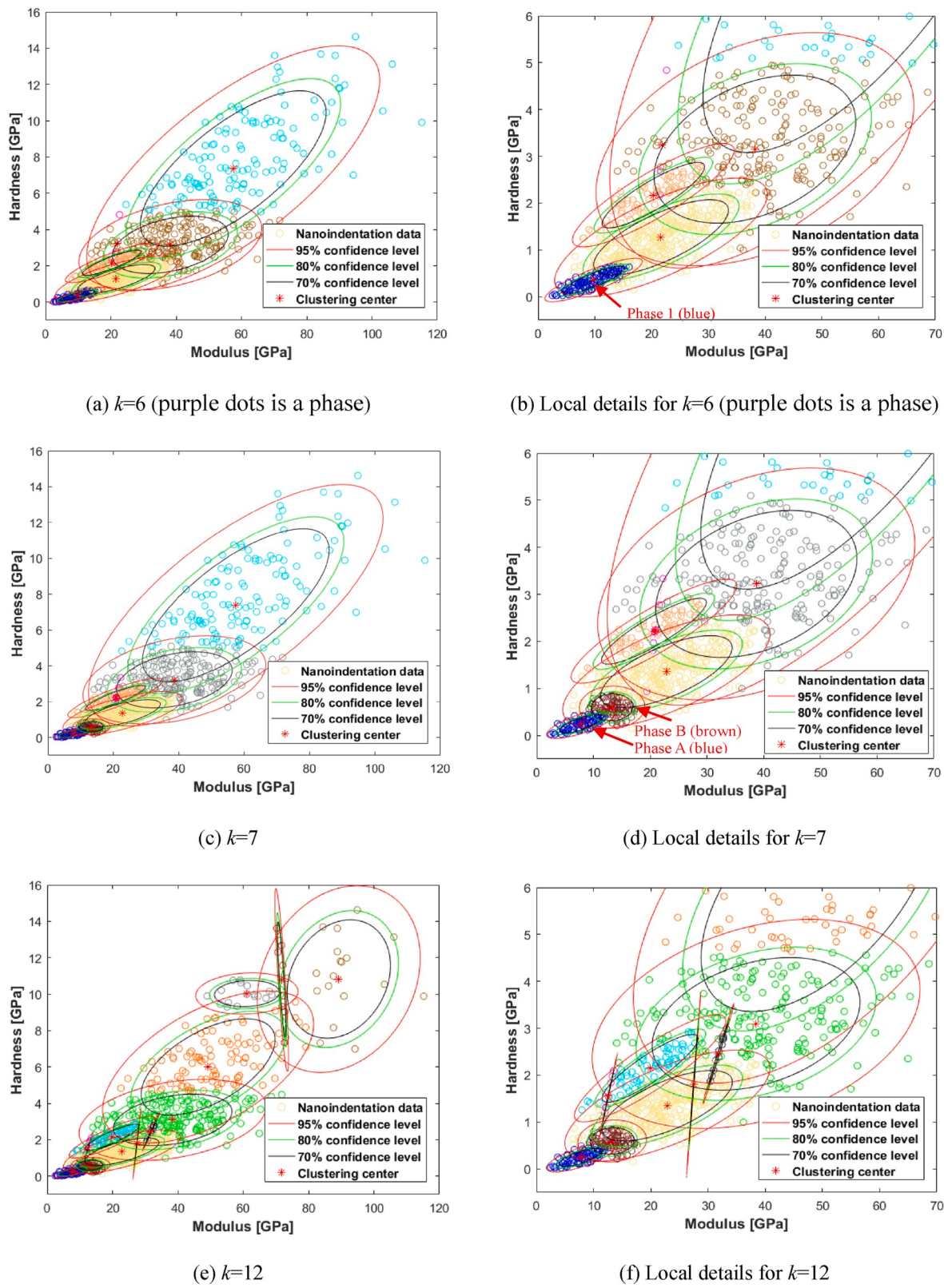
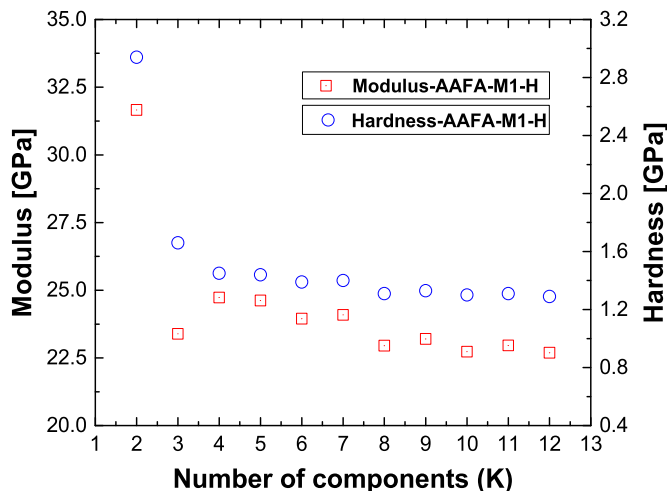
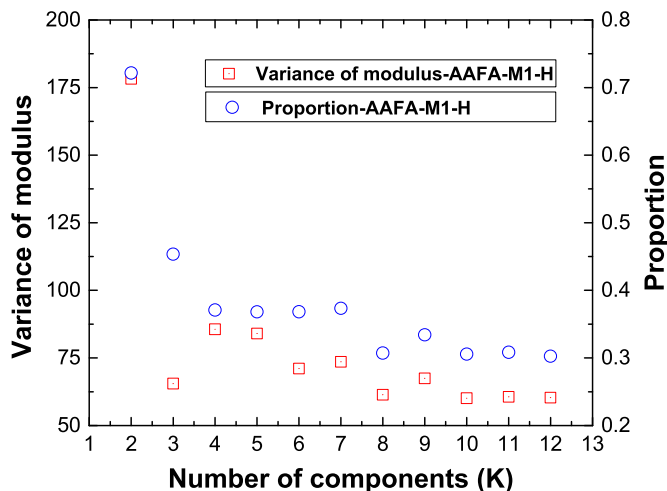


Fig. 4. Deconvolution of nanoindentation data (elastic modulus and hardness) for AAFA-M0-H.



(a) Nano/micromechanical properties of AAFA-M1-H



(b) Variance and proportion of AAFA-M1-H

Fig. 5. The first deconvolution results for AAFA-M1-H.

gel phase lasts more than three models, then the final properties of the gel phase are determined by the average value of the first three results to reduce the impact of uncertainty (average all gel phases when less than 3). Considering the fact that geopolymers at least contains gel, mixed phase, and unreacted fly ash, the possible gel phase should be selected from the model by at least 3 components. For AAFA-M1-S, it is the average result from 5 components model to 7 components model as listed in the last row of Table 3. Correspondingly, it is the average result of 3 components model to 5 components model for AAFA-M0-H, 12-3 components model to 12-5 components model for AAFA-M1-H and 4 components model to 6 components model for AAFA-M1.5-H. The phase in the 3 components model of AAFA-M1.5-H is not accepted as the gel phase as it has large variance and a large range of variation of both elastic modulus and hardness.

5.2. Evaluation of deconvolution error

In order to compare the nano/micromechanical properties of N-A-S-H in different geopolymers, one of the key issues is to evaluate the errors generated from the analytical technique itself. The first error should be the average method we adopted to represent the nano/micromechanical properties of gels. Illustrated by the case of AAFA-M1-S, the possible

elastic modulus of gel for it is 11.20, 11.18 or 10.76 GPa. For the average value of 11.05 GPa adopted, the corresponding deviation is 0.15, 0.13 or -0.29 GPa, as shown in Fig. 8. For all these samples, the maximum possible deviations are 0.99 GPa for elastic modulus, 0.09 GPa for hardness and 4.83% for proportion. The average value of all those deviations (absolute value) for elastic modulus, hardness, and proportion are 0.44 GPa, 0.04 GPa, and 1.37%, respectively.

Another possible error can be ascribed to the test data, although the number of points (Nine grids) we tested is more than conventional research. The number of grids was increased to 18 for AAFA-M0-H to check if there are significant different results for the properties obtained from 9 grids and 18 grids. Since this study aims at the gel phase only, the additional grids were intentionally put on the areas that very rich in gel to provide more data for the analysis of gel. Some typical results for AAFA-M0-H based on 18 grids are compared with the results from 9 grids and shown in Fig. 9. The micromechanical results from models are (11.08, 0.57) for 3 components and (9.43, 0.42) for 4 components, respectively. There are close to the corresponding values obtained from the deconvolution of 9 grids as given in Table 4. When increasing the number of components, there will be no more similar gel phase. Namely, the average properties for N-A-S-H gel based on 18 grids are (10.26, 0.50).

One special phenomenon for AAFA-M0-H is the presence of two phases when the number of components is more than 7, while both of these two phases have a considerable proportion. For the sake of comparison, the 7 components model based on 18 grids is provided in Fig. 9 (g) and (h). Similar to that in Fig. 4, there are also two phases. The blue phase and the brown phase have the properties of (6.99, 0.25) and (11.27, 0.56), respectively. It indicates that the two phases are not generated due to the limited test data. It is easy to track that these two phases are mainly decomposed by the gel phase in models that have few components, although some points are removed or included during this process. The average properties of these two phases in the 7 component model based on both 9 grids and 18 grids are obtained by the cluster of data for each phase. As shown in Fig. 9, the nanoindentation data that belong to the phases with nano/micromechanical properties of (6.99, 0.25) and (11.27, 0.56) are clustered into blue points and brown points according to the maximum posterior probability. The blue points and brown points are collected and plotted in Fig. 10(a) and (b), with their average value denoted by the clustering center, which are (6.75, 0.23) and (11.32, 0.55), respectively. Namely, the clustered data can well represent the estimated phase in the deconvolution of AAFA-M0-H based on 18 grids. Then, the blue points and brown points are combined together. The average properties of all those points are (9.60, 0.43) as shown in Fig. 10(c). Similarly, the average properties of all those points in AAFA-M0-H based on 9 grids are (10.66, 0.42). The average properties of blue and brown phase are similar in models with different grid numbers. Moreover, the average properties of these two phases are very close to the properties of the gel phase. It is possible that the blue phase is the gel with higher porosity than the brown phase.

The errors result from limited test data are summarized in Fig. 10(d). For the elastic modulus and hardness of N-A-S-H we study, the deviation of results is just -0.24 and 0.09 GPa, respectively. Taking into account the above errors caused by the average method to determine the properties of gel phase, the approximate errors for elastic modulus and hardness are 0.68 and 0.13 GPa. Meanwhile, the maximum deviations are obtained as 1.23 GPa for elastic modulus and 0.18 GPa for hardness. One thing to note is the results are based on the sum of the absolute values that would enlarge the evaluation of the errors. Namely, the positive and negative errors do not cancel each other out.

5.3. Correlation and difference of different statistical techniques

For the LSE method that generally used to fit the frequency density histogram for deconvolution analysis, it is known to depend on the bin size. The correlation and difference of the LSE and MLE methods are

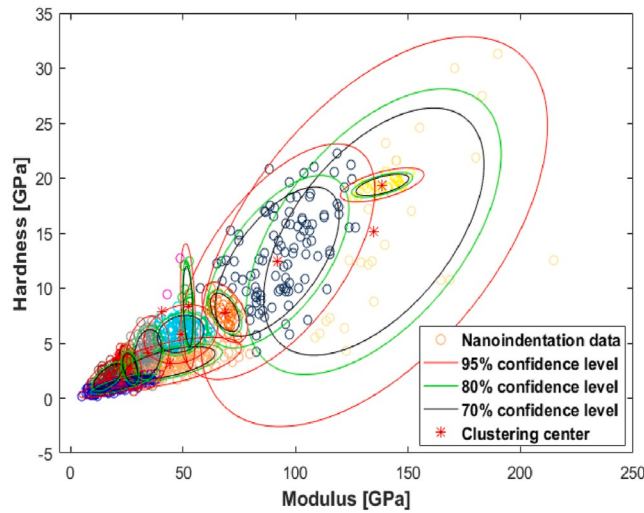
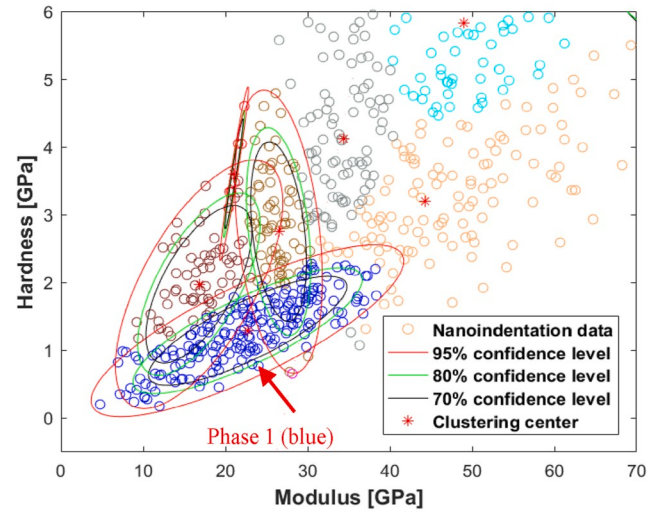
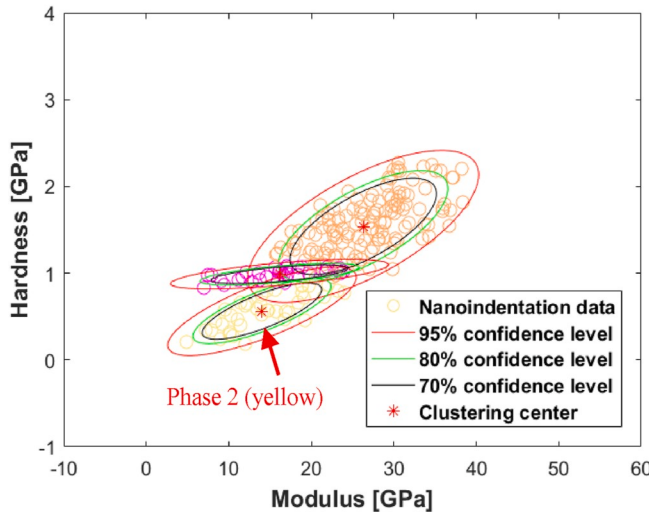
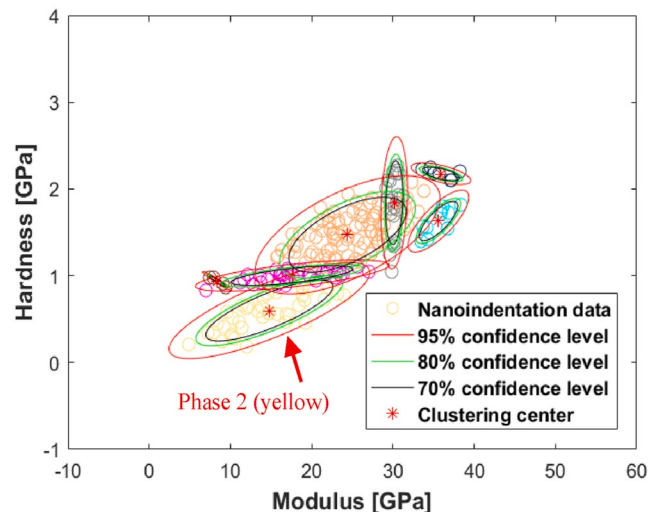
(a) 1st deconvolution with $k=12$ (b) Local details for $k=12$ (c) 2nd deconvolution with $k=3$ (12-3)(d) 2nd deconvolution with $k=7$ (12-7)**Fig. 6.** The second deconvolution for AAFA-M1-H.

Table 5

Deconvolution result for clustered data belong to stable phase when k is 12 (AAFA-M1-H, clustered yellow points for $k = 12\text{-}3$ and $12\text{-}7$).

k	M [GPa]	H [GPa]	f	BIC	C		
					C11	C12	C22
					=	C21	
12-1	22.71	1.29	100.00% (30.25%)	1473.28	58.54	3.14	0.25
12-2	22.20	1.24	93.54% (28.30%)	1460.87	58.45	2.96	0.22
12-3	14.03	0.56	19.90% (6.02%)	1446.38	16.84	0.75	0.04
12-4	14.19	0.58	21.06% (6.37%)	1435.05	16.90	0.79	0.05
12-5	14.67	0.58	20.17% (6.10%)	1425.61	19.83	0.84	0.04
12-6	15.26	0.63	19.99% (6.05%)	1419.11	19.36	0.81	0.04
12-7	14.79	0.60	22.74% (6.88%)	1416.02	19.68	0.91	0.05
Ave_12_3-5	14.30	0.57	20.38% (6.16%)	—	17.86	0.79	0.04

Note: the fraction without brackets is the proportion of the component to all components in the second time of deconvolution, and the fraction within brackets is the proportion of the component to all components in original AAFA reaction system.

discussed by the hardness histogram of AAFA-M1-S. The possible N-A-S-H gel phase of AAFA-M1-S starts to appear in the model with 5 components and decompose into two phases in the model with 10 components. The possible gel would exist in models with 5–9 components. However, as displayed in Fig. 11, any model could match the histogram if suitable bin size is set for the histogram. If the bin size is more than 0.28, it is not possible to obtain the hardness of N-A-S-H gel, denoted by the green peak in Fig. 11(b) and (c), as there is no corresponding peak in the histogram. The large green peak in Fig. 11(a) would be misidentified as the N-A-S-H. Generally, the bin size set in exiting studies is more than 0.28 and the number of components adopted is 4. In that case, the final results should be from a mixed phase instead of N-A-S-H gel. When the bin size is small to around 0.12, as can be clearly observed from Fig. 11(c) and (d), the model with 10 components can even better match the histogram than the model with 9 components. Consequently, the properties of N-A-S-H would be erroneously derived from the 10 components model.

For the GMM estimated by the MLE method, reasonably increasing the number of components enables the model to reflect more details of the distribution of the collected data. Bin size plays a similar role in the histogram. Smaller bin size contributes to revealing more information on the collected data. Therefore, for the models with increased phases, there are histograms with decreased bin sizes that can match them. However, for both of the number of components and bin size, the inappropriate parameters would lead to either mixed phase ($k = 4$) or sub-phases ($k = 10$). For the MLE method adopted, the gel phase could be determined by empirical knowledge of multiple parameters within a few models with a different number of components. For LSE method, the bin size is hard to set reasonably, since it is a continuous number with an infinite range of values. Besides, the suitable bin size would be affected by lots of factors, such as features of the sample and the number of test data. For the same bin size, a small number of test data would be no more able to form a neat and identifiable histogram for fitting.

5.4. Nano/micromechanical properties of N-A-S-H gel in geopolymers

The properties of the gel phases in this study are summarized in Table 7. It is obvious that the AAFA-M1-H sample has the highest nano/micromechanical properties while the AAFA-M0-H has the lowest one. The properties of the AAFA-M1-S are just slightly higher than the AAFA-

M0-H and modestly lower than the AAFA-M1.5-H. As estimated above, the possible errors for elastic modulus and hardness are around 0.68 and 0.13 GPa, respectively. Even in the most unfavorable situation, where the larger one has been overestimated and the smaller one has been underestimated (deviation of 1.36 and 0.26 GPa), one still can point that the elastic modulus of AAFA-M1-H is larger than the AAFA-M0-H and AAFA-M1-S, and AAFA-M1.5-H is larger than AAFA-M0-H. In our other research, higher elastic modulus and hardness of 15.46 and 0.73 GPa than AAFA-M1-H were obtained for geopolymers with similar mix design but higher alkali concentration of 10%. Thus, the statistical nano-indentation results suggest that the nano/micromechanical properties of N-A-S-H gel should vary with the samples, but just in a very small range. The variation range of the elastic modulus obtained here is smaller than that of other studies by the LSE method [29,30].

5.5. Mechanism of characteristics of nano/micromechanical properties

The nano/micromechanical properties of N-A-S-H gels obtained in this study are similar but slightly lower than that of LD C-S-H gel [22]. Besides, the proportion of it is also lower than reported for both N-A-S-H [27,28] and LD C-S-H [50]. In fact, there is an important factor that would influence the test results but hasn't been considered in existing nanomechanical test research of N-A-S-H gel, namely, the presence of crystals. Although the study by the XRD shown in Fig. 12 doesn't detect any new crystals when compared with raw material fly ash, it can't eliminate the possibility that the crystals significantly affect the results. In the activation process, crystals are hard to react which would then be surrounded by the generated gel. Evidence can be found by the micro to nanoscale observation of N-A-S-H gel displayed in Fig. 13. Slender crystals can be observed clearly in Fig. 13(a). Additionally, for the gel near the clustered crystals, the magnified photo in Fig. 13(b) indicates that there are also lots of crystals in the gel. Higher magnification observations were conducted at lots of other locations of the sample. Although there is gel without recognizable crystal as shown in Fig. 13(c), nano to sub-micron crystals can be found to embed in gel in some other locations. The presence of crystals in the involved range of nano-indentation would significantly enhance the mechanical properties and then identified as the mixed phase in deconvolution analysis. It should be the main reason responsible for the low proportion of the gel obtained. For almost all of the samples, there is a phase with elastic modulus slightly more than 20 GPa and hardness slightly more than 1 GPa. It can be typically found in Fig. 3(f) for AAFA-M1-S (yellow phase), Fig. 4(b) for AAFA-M0-H (yellow phase), Fig. 6(b) for AAFA-M1-H (blue phase), Fig. 7(b) for AAFA-M1.5-H (blue phase, 21.43 GPa, 1.52 GPa). For AAFA-M0-H based on 18 grids, the majority of the new test points from the additional nanoindentation grids are intentionally not put on unreacted fly ash. Hence, the test data would concentrate on the region with smaller nano/micromechanical properties. The part of this mixed phase with large mechanical properties would be lost in the deconvolution due to the small proportion, resulting in the slightly smaller of the mechanical properties of it. The same consideration could possibly also be applied for AAFA-M1.5-H. The maximum proportion of it may be ascribed to the grids. Some of them happen to be in gel-rich areas. This mixed phase also shows small properties when k is large.

The final N-A-S-H gel phase is separated from the part of this kind of mixed phase where it has the lowest mechanical properties. This phase may be mainly a mixture of crystals and gels, and have a small fraction of other inclusions. Firstly, the "big phase" can be found in all samples with similar properties which mean it may be a stable phase that exists in AAFA rather than a mixture of gel phase with random inclusions. Besides, the nano/micromechanical properties of this kind of mixed phase are close and a bit lower than the agglomeration of C-S-H and CH crystal identified in Portland cement paste [36], which is plausible to be the mixture of N-A-S-H and crystals as the nano/micromechanical properties of N-A-S-H is also a bit lower than the LD C-S-H. This kind of mixed phase has lower mechanical properties than other phases. This

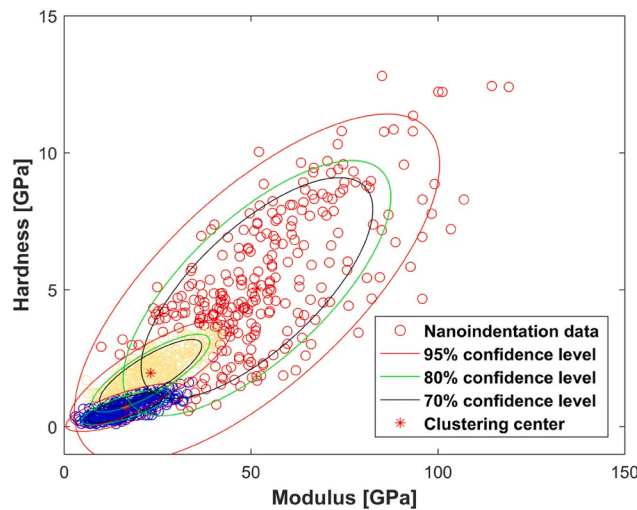
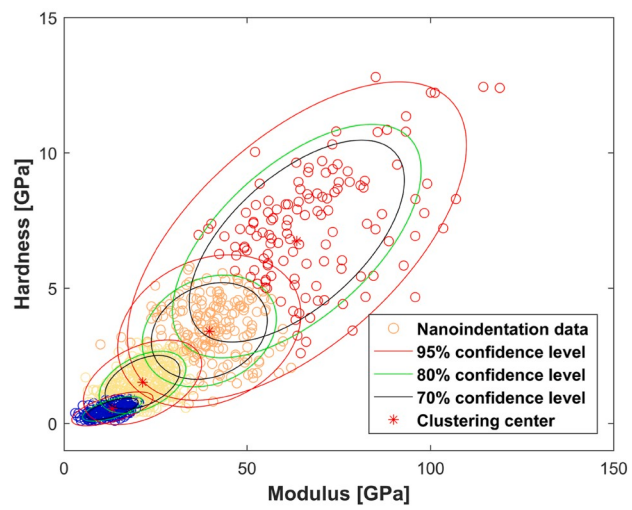
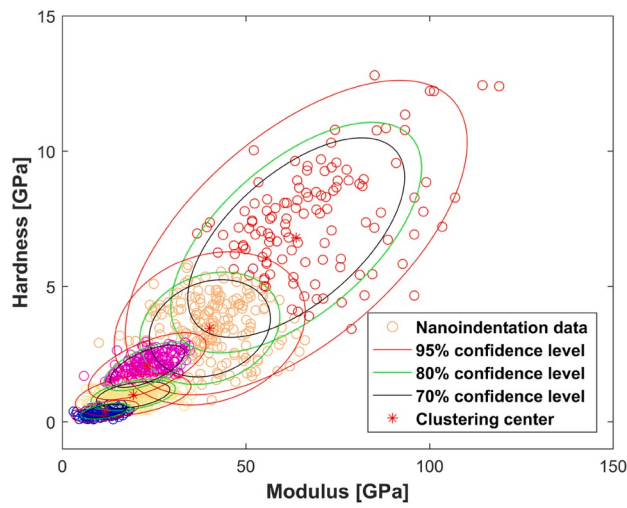
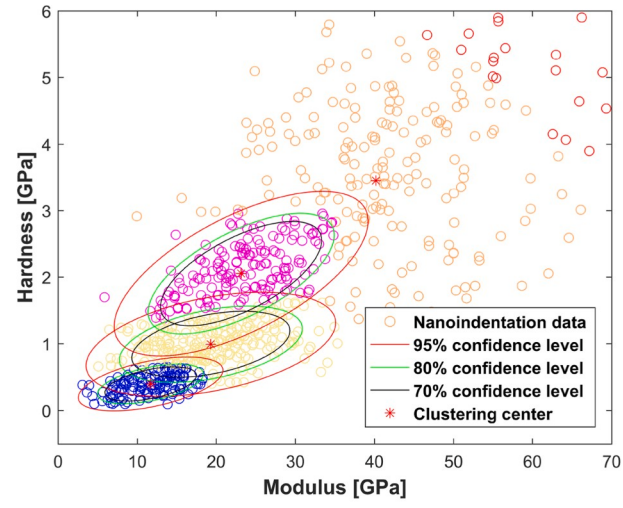
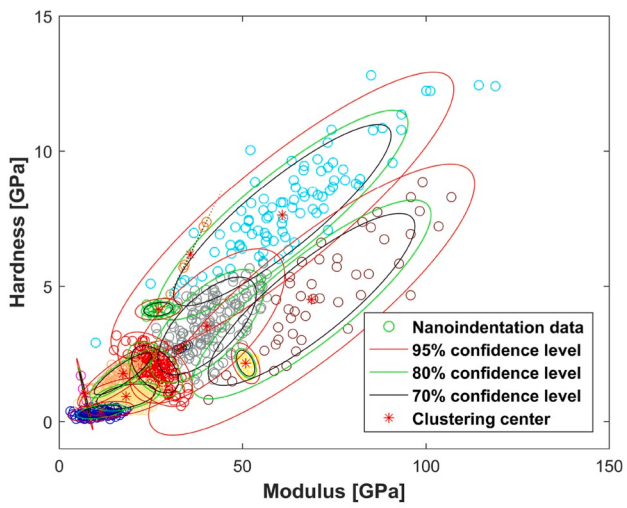
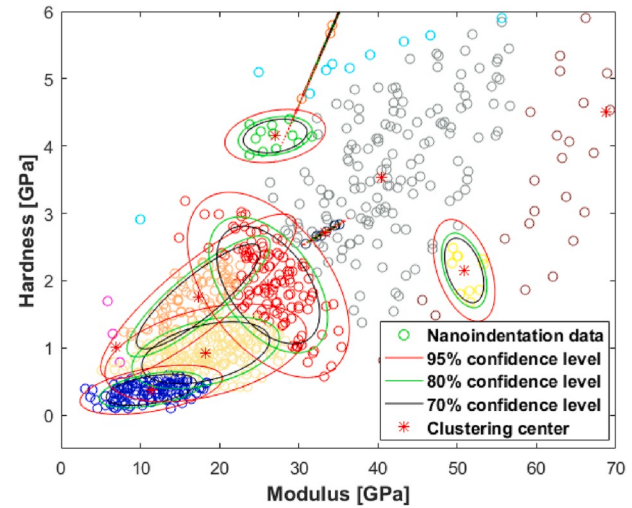
(a) $k=3$ (b) $k=4$ (c) $k=5$ (d) Local details for $k=5$ (e) $k=12$ (f) Local details for $k=12$

Fig. 7. Deconvolution of nanoindentation data (elastic modulus and hardness) for AAFA-M1.5-H.

Table 6

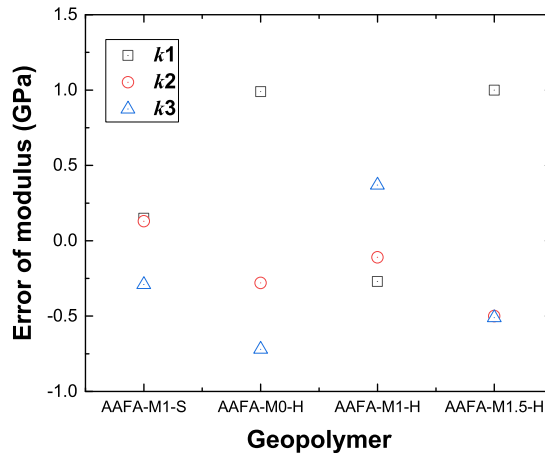
Deconvolution result for AAFA-M1.5-H (clustered blue points).

k	M [GPa]	H [GPa]	f	BIC	C		
					C11	C12 = C21	C22
2	18.68	1.19	60.21%	9330.89	54.53	3.96	0.55
3	16.57	0.71	33.69%	9185.27	43.51	1.79	0.13
4	13.21	0.54	22.40%	9135.45	20.70	0.76	0.07
5	11.71	0.40	15.21%	9088.36	14.02	0.31	0.03
6	11.70	0.40	15.10%	9066.53	13.98	0.31	0.03
7	11.72	0.40	15.40%	9048.99	14.02	0.31	0.03
8	11.36	0.39	14.63%	9033.79	12.81	0.27	0.03
9	11.72	0.40	15.41%	9026.87	14.00	0.31	0.03
10	11.37	0.38	13.81%	9011.51	13.50	0.26	0.02
11	11.58	0.39	13.95%	8996.77	12.14	0.26	0.02
12	11.37	0.38	13.62%	8995.79	13.53	0.26	0.02
Ave_4-	12.21	0.45	17.57%	–	16.23	0.46	0.04
6							

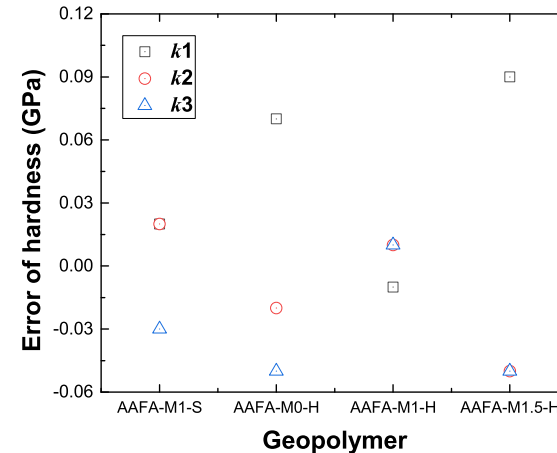
Note: The numbers in the column of “M” and “H” refer to mean value of elastic modulus and hardness, respectively. f is the proportion of the phase. C is covariance matrix, where C11 is the variance of elastic modulus, C22 is the variance of hardness and C12 is the covariance of modulus and hardness.

may be caused by the small scale of the crystals and different mechanical properties of it compared with other unreacted particles that come from fly ash.

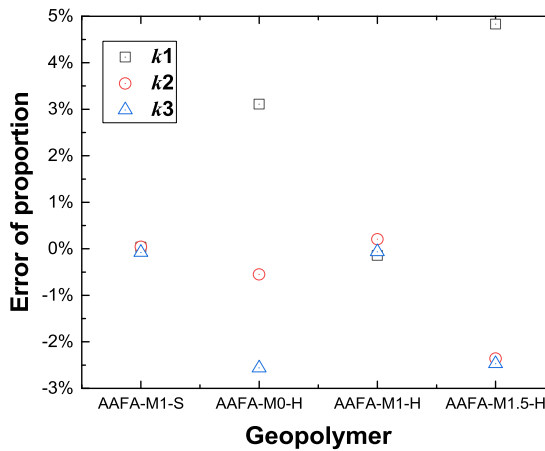
As shown in Fig. 13, the microstructure of N-A-S-H is found to be looser than that normally known for C-S-H gel, which may be the reason for lower nano/micromechanical properties of N-A-S-H gel, and then the generally lower macro performance of fly ash-based geopolymers. In terms of the nano/micromechanical properties in different geopolymers, the variation may be affected by both the nanomechanical properties of the gel particles and the nanoscale pores. For the study of C-S-H in Portland cement paste, Jennings [51] proposed a simplified model to represent the microstructure of C-S-H. Basic spherical blocks with size about 2 nm cluster together to form globules and then the globules pack together to form LD and HD C-S-H structures. This model is further modified using packing structure with around 5 nm globules as the basic unit [32] to help the understanding of the microstructural changes associated with drying and heat curing. The globules are considered to have intrinsic packing density. The geopolymers gel is also formed by the packing of primary globular polymeric entities of several nanometers [52], which can't be observed in Fig. 13 due to the limited resolution of SEM. The globular polymeric entities form gel particles with the sizes of dozens of nanometers, while the gel particles are not always tightly integrated as shown in Fig. 13(c) and (d). The defects and pores between gel particles would be a factor affecting the nano/micromechanical properties detected. The gel particles are governed by the globular polymeric entities and their packing density, while the stiffness of polymeric entities may be affected at least by its maturity and chemical structure.



(a) Error of modulus



(b) Error of hardness



(c) Error of proportion

Fig. 8. Errors result from the average method to determine the nano/micromechanical properties of gel.

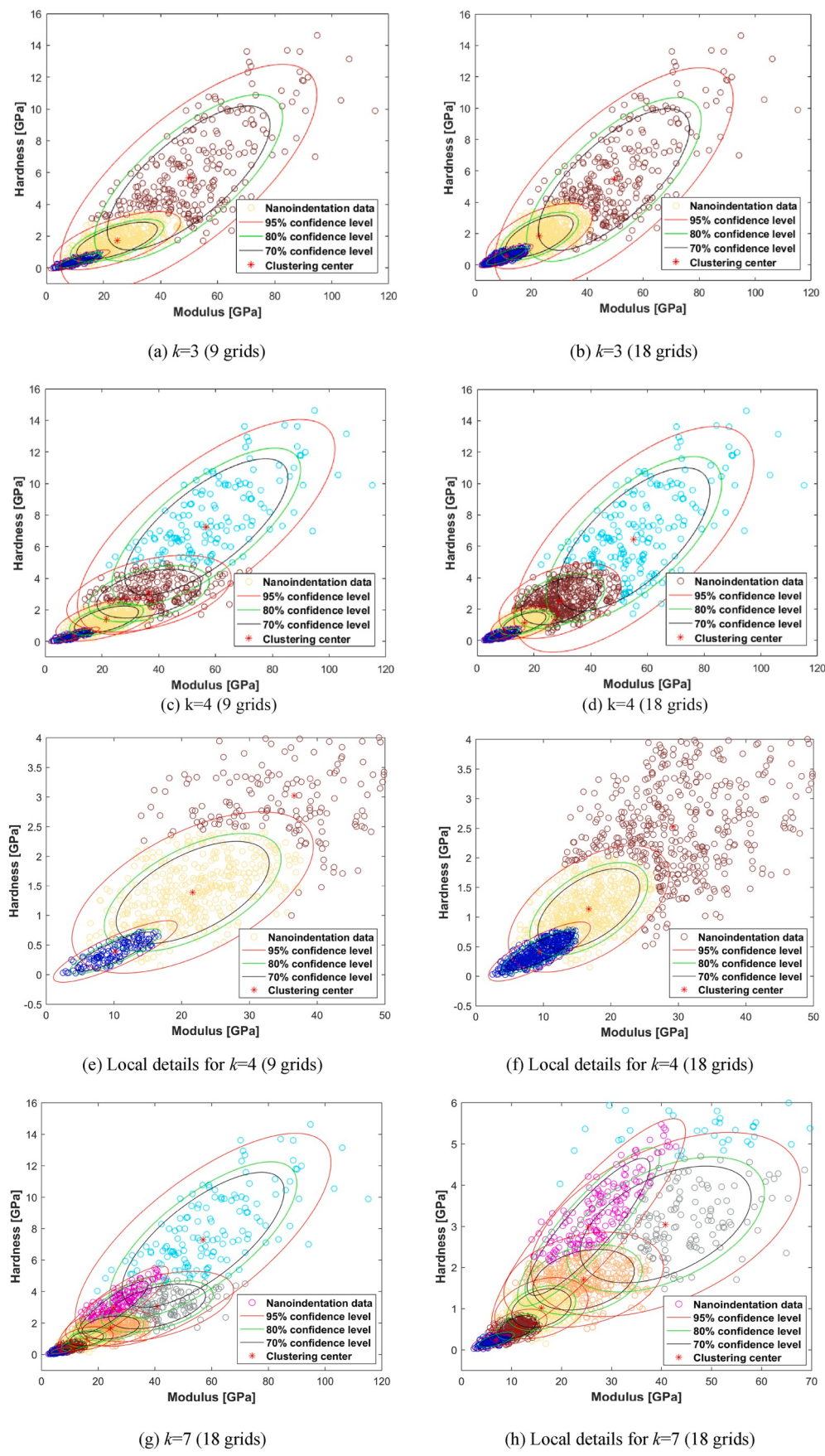
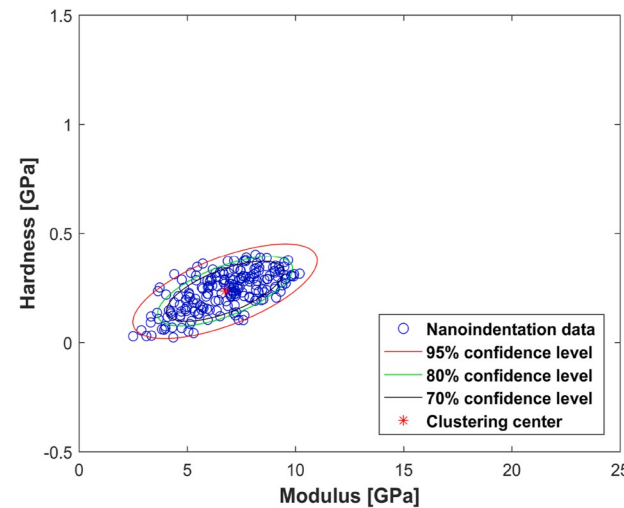
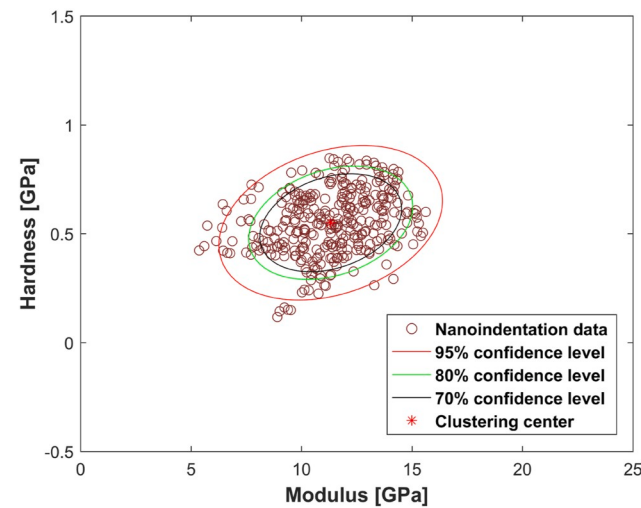


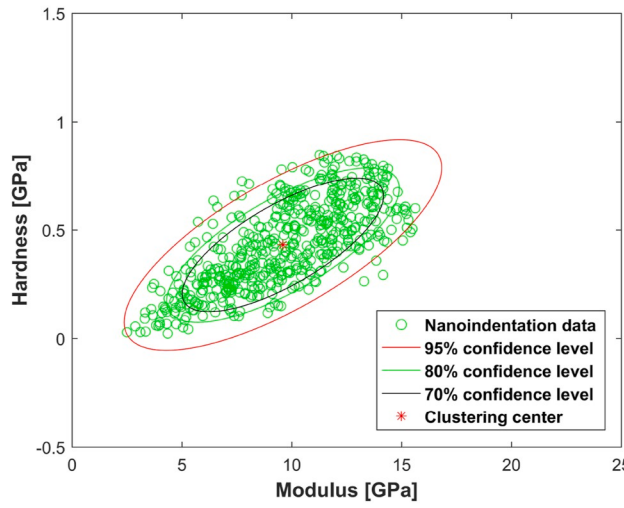
Fig. 9. Errors result from the limited test data of statistical nanoindentation.



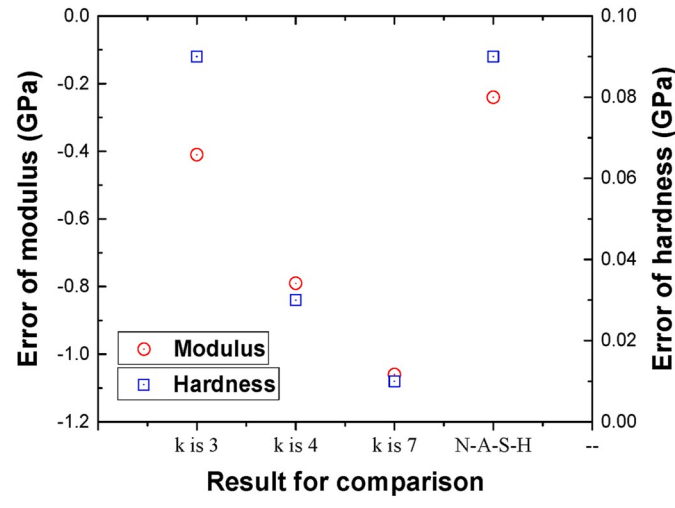
(a) Clustered data for estimated phase with M of 6.99
and H of 0.25



(b) Clustered data for estimated phase with M of 11.27 and
 H of 0.56



(c) Average properties of two decomposed phases



(d) Deviation of results between deconvolution of 9 grids
and 18 grids data

Fig. 10. Average properties of the decomposed phases in the 7 component model of AAFA-M0-H (18 grids), and results of error evaluation.

The different maturity, and the different composition and chemical structure of the N-A-S-H gel are considered by Ma et al. [30] as the main reasons that account for the constant elastic's modulus in the study by Nêmeček et al. [27] but varied elastic modulus in the study by Ma et al. [30]. The polymerization process of AAFA is very slow and heat curing is usually used to accelerate it. For ambient cured AAFA and heat cured AAFA with different curing temperature, the difference between their 28-day compressive strength and longer time compressive strength is quite different [53–55] and larger than the difference in the Portland cement paste, which means that at 28 days, the samples have significantly different reaction degree under different curing conditions. The different maturity would induce different stiffness of polymeric entities, the gel particles and then the nano/micromechanical properties of the N-A-S-H gel. This is considered as the dominant reason for the

significantly smaller properties of AAFA-M1-S than AAFA-M1-H. As for the influence of the composition and chemical structure of the gel phase, Georgios and Ulm [56] found that the C-S-H decalcification would cause remarkable degradation of elastic modulus of C-S-H gel. Additionally, the indentation modulus and hardness of the synthetic C-S-H would change with the Ca/Si molar ratio [57]. For geopolymers, within a suitable range, the increase of silica content may result in the increase of the fully condensed tetrahedral aluminosilicate network structures and then the strength of the geopolymers due to the higher strength of Si–O–Si bonds than the Si–O–Al bonds [52]. These results or theoretical basis indicate that the globular polymeric entities themselves may have different stiffness when chemical structure changed significantly. NaOH activated fly ash normally has lower macro strength than the alkali-silicate activated fly ash with similar mixture and condition.

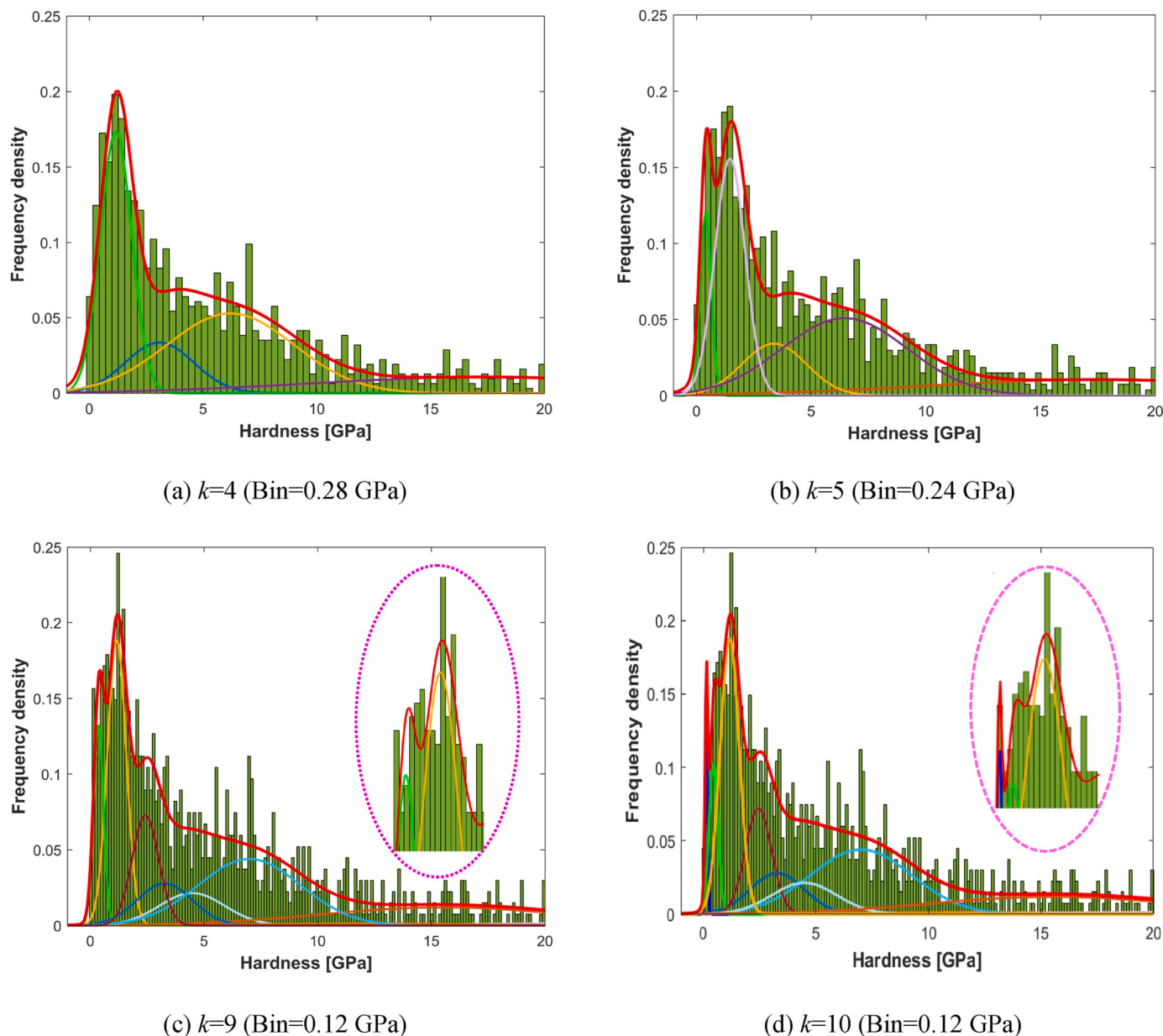


Fig. 11. Compare of PDF with hardness frequency histogram for AAFA-M1-S.

Table 7
Properties of N-A-S-H in geopolymers with different silica modulus under different curing conditions.

Samples	k	M [GPa]	H [GPa]	f	C		
					C11	C12=C21	C22
AAFA-M1-S	Ave_5-7	11.05	0.40	7.24%	12.63	0.57	0.06
AAFA-M0-H	Ave_3-5	10.50	0.41	14.66%	15.42	0.76	0.05
AAFA-M1-H	Ave_12_3-5	14.30	0.57	6.16%	17.86	0.79	0.04
AAFA-M1.5-H	Ave_4-6	12.21	0.45	17.57%	16.23	0.46	0.04

Provis et al. [40] proposed that larger crystals in NaOH activated fly ash are hard to pack densely within the binder phase, which could be one of the reasons for its low macro strength. The lowest nanoindentation results for AAFA-M0-H can provide another reason that the N-A-S-H gel in NaOH activated fly ash would have lower micro-strength than others. These two factors work together to make the lower macro strength of NaOH activated fly ash.

6. Conclusions

In this study, the nano/micromechanical properties of sodium aluminosilicate hydrate (N-A-S-H) gel in alkali-activated fly ash (AAFA) geopolymer under different silica modulus and curing conditions are investigated by deconvolution of grid nanoindentation data with maximum likelihood estimation method. The following conclusions can be drawn up:

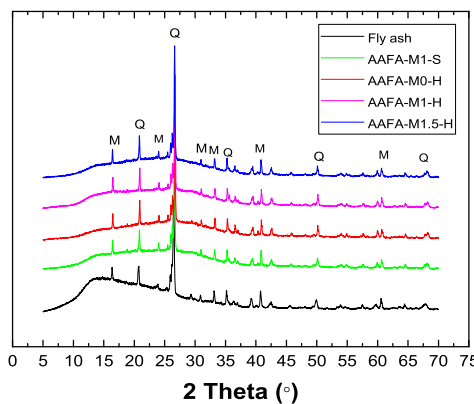


Fig. 12. X-ray diffractogram of geopolymer pastes.

- (1) Mixed phases and sub-phases are typical spurious phases in geopolymers. It is virtually impossible to reconcile these two kinds of spurious phases to obtain the accurate nano/micromechanical properties of each real component by statistical nanoindentation. A compromise approach was proposed, which ensures the accuracy of the gel phase by intentionally introducing spurious phases for other components.
- (2) The errors generated from the analytical technique itself were estimated from the two aspects of the average method adopted, and the number of the experimental data. The average deviation of elastic modulus and hardness introduced by the average method are 0.44 GPa, 0.04 GPa, respectively. Correspondingly, the number of test data would bring the errors of -0.24 GPa and 0.09 GPa.
- (3) For the GMM estimated by MLE method, reasonably increasing the number of components enables the model to reflect more details of the distribution of the collected data. Bin size plays a similar role in the histogram. When increasing the number of

phases in the model, there are hardness histograms with decreased bin sizes that can match them. Different from the MLE method where multiple parameters could be referenced to determine the gel in a few models, the appropriate bin size is practically impossible to be determined from the infinite range of values.

- (4) The nano/micromechanical properties obtained for geopolymers vary in a minor range of 10.50–14.30 GPa for elastic modulus and 0.40–0.57 GPa for hardness. The highest nano/micromechanical properties were achieved by AAFA-M1-H. Both AAFA-M0-H and AAFA-M1-S show significantly lower properties. The variation may be affected by both the nanomechanical properties of the gel particles and the nanoscale pores between them. The formal one would be determined at least by its maturity and chemical structure.
- (5) The intermixing of crystal gels was observed under high-resolution SEM. The interaction of them in the involved range results in a mixed phase in deconvolution, which largely decreased the proportion of N-A-S-H gel obtained. Compared to C-S-H, the looser structure of N-A-S-H should be one of the reasons for its inferior nano/micromechanical properties.

Declaration of competing interest

The authors declare that they have no known competing financial interests or personal relationships that could have appeared to influence the work reported in this paper.

CRediT authorship contribution statement

Zhiyu Luo: Formal analysis, Data curation, Methodology, Validation, Writing - original draft, Writing - review & editing, Software. **Wengui Li:** Conceptualization, Formal analysis, Data curation, Validation, Investigation, Writing - original draft, Writing - review & editing, Funding acquisition, Supervision, Project administration, Resources.

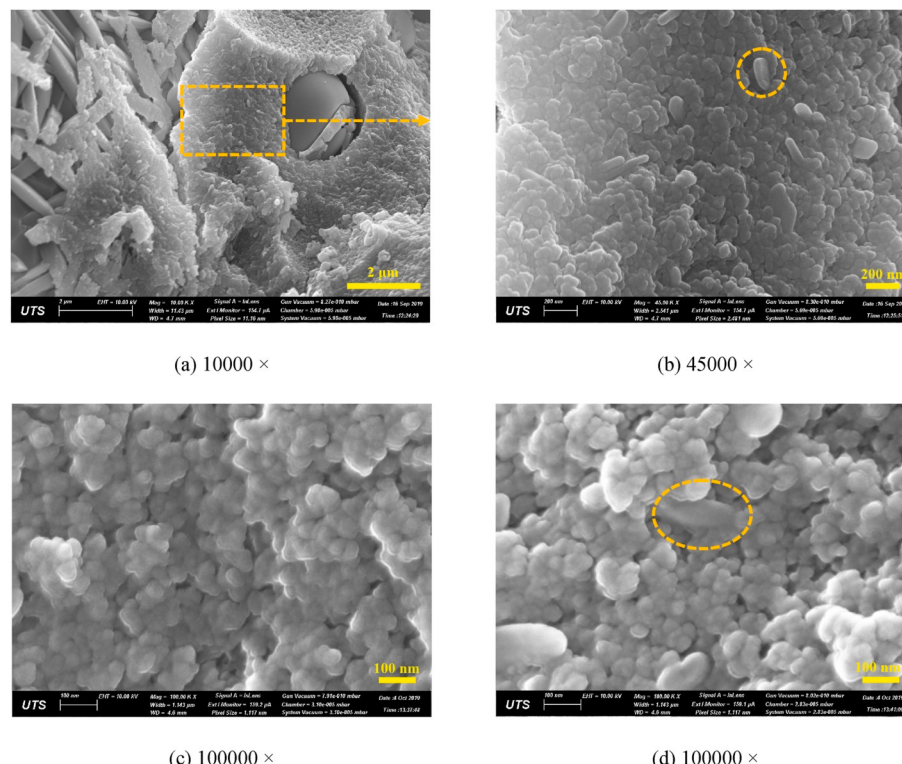


Fig. 13. Microstructure of N-A-S-H gel in AAFA.

Yixiang Gan: Methodology, Validation, Writing - original draft, Writing - review & editing, Software. **Kavya Mendum:** Formal analysis, Investigation, Writing - review & editing. **Surendra P. Shah:** Formal analysis, Investigation, Writing - review & editing.

Acknowledgements

All authors appreciate the support from the Australian Research Council (DE150101751), University of Technology Sydney Research Academic Program at Tech Lab (UTS RAPT), and University of Technology Sydney Tech Lab Blue Sky Research Scheme. The first author also would like to thank the Australian Government Research Training Program Scholarship.

References

- [1] Fang G, Zhang M. Multiscale micromechanical analysis of alkali-activated fly ash-slag paste. *Cem Concr Res* 2020;135:106141.
- [2] Luo Z, Li W, Gan Y, Mendum K, Shah S. Applying grid nanoindentation and maximum likelihood estimation for N-A-S-H gel in geopolymer paste: Investigation and discussion. *Cem Concr Res* 2020;135:106112.
- [3] Li N, Shi C, Zhang Z, Wang H, Liu Y. A review on mixture design methods for geopolymer concrete. *Compos B Eng* 2019;178:107490.
- [4] Zhang Z, Wang H, Zhu Y, Reid A, Provis JL, Bullen F. Using fly ash to partially substitute metakaolin in geopolymer synthesis. *Appl Clay Sci* 2014;88:194–201.
- [5] Yan L, Kasal B, Huang L. A review of recent research on the use of cellulosic fibres, their fibre fabric reinforced cementitious, geo-polymer and polymer composites in civil engineering. *Compos B Eng* 2016;92:94–132.
- [6] Scrivener KL, Kirkpatrick RJ. Innovation in use and research on cementitious material. *Cement Concr Res* 2008;38(2):128–36.
- [7] Zhang Z, Provis JL, Reid A, Wang H. Geopolymer foam concrete: an emerging material for sustainable construction. *Construct Build Mater* 2014;56:113–27.
- [8] Nikolić V, Komiljenović M, Džunuzović N, Ivanović T, Miladinović Z. Immobilization of hexavalent chromium by fly ash-based geopolymers. *Compos B Eng* 2017;112:213–23.
- [9] Zhang Z, Yao X, Zhu H. Potential application of geopolymers as protection coatings for marine concrete: I. Basic properties. *Appl Clay Sci* 2010;49(1–2):1–6.
- [10] Zhang Z, Provis JL, Reid A, Wang H. Fly ash-based geopolymers: the relationship between composition, pore structure and efflorescence. *Cement Concr Res* 2014;64:30–41.
- [11] Luo Z, Li W, Wang K, Shah SP. Research progress in advanced nanomechanical characterization of cement-based materials. *Cement Concr Compos* 2018;94: 277–95.
- [12] Tian C, Feng Y, Chu G, Lu Y, Miao C, Ning N, et al. Interfacial nanomechanical properties and chain segment dynamics of fibrillar silicate/elastomer nanocomposites. *Compos B Eng* 2020;193:108048.
- [13] Schuh CA. Nanoindentation studies of materials. *Mater Today* 2006;9(5):32–40.
- [14] Zhang H, Šavija B, Luković M, Schlangen E. Experimentally informed micromechanical modelling of cement paste: an approach coupling X-ray computed tomography and statistical nanoindentation. *Compos B Eng* 2019;157: 109–22.
- [15] Han Q, Geng Y, Setchi R, Lacan F, Gu D, Evans SL. Macro and nanoscale wear behaviour of Al-Al2O3 nanocomposites fabricated by selective laser melting. *Compos B Eng* 2017;127:26–35.
- [16] Li W, Xiao J, Kawashima S, Shekhawat GS, Shah SP. Experimental investigation on quantitative nanomechanical properties of cement paste. *ACI Mater J* 2015;112: 229–38.
- [17] Hu C, Ruan Y, Yao S, Wang F, He Y, Gao Y. Insight into the evolution of the elastic properties of calcium-silicate-hydrate (CSH) gel. *Cement Concr Compos* 2019;104: 103342.
- [18] Khedmati M, Kim Y-R, Turner JA. Investigation of the interphase between recycled aggregates and cementitious binding materials using integrated microstructural-nanomechanical-chemical characterization. *Compos B Eng* 2019;158:218–29.
- [19] Li W, Kawashima S, Xiao J, Corr DJ, Shi C, Shah SP. Comparative investigation on nanomechanical properties of hardened cement paste. *Mater Struct* 2016;49(5): 1591–604.
- [20] Zhu W, Hughes JJ, Bicanic N, Pearce CJ. Nanoindentation mapping of mechanical properties of cement paste and natural rocks. *Mater Char* 2007;58(11–12): 189–98.
- [21] Allison PG, Weiss Jr C, Moser RD, Diaz A, Rivera OG, Holton SS. Nanoindentation and SEM/EDX characterization of the geopolymer-to-steel interfacial transition zone for a reactive porcelain enamel coating. *Compos B Eng* 2015;78:131–7.
- [22] Hu C, Li Z. A review on the mechanical properties of cement-based materials measured by nanoindentation. *Construct Build Mater* 2015;90:80–90.
- [23] Vandamme M, Ulm F-J. Nanoindentation investigation of creep properties of calcium silicate hydrates. *Cement Concr Res* 2013;52:38–52.
- [24] Jones CA, Grasley ZC. Short-term creep of cement paste during nanoindentation. *Cement Concr Compos* 2011;33(1):12–8.
- [25] Němcéek J, Králik V, Šmilauer V, Polívka L, Jäger A. Tensile strength of hydrated cement paste phases assessed by micro-bending tests and nanoindentation. *Cement Concr Compos* 2016;73:164–73.
- [26] Soliman EM, Aboubakr SH, Taha MMR. Estimating fracture toughness of C-S-H using nanoindentation and the extended finite element method. *Int J Adv Eng Sci Appl Math* 2017;9(3):154–68.
- [27] Němcéek J, Šmilauer V, Kopecký L. Nanoindentation characteristics of alkali-activated aluminosilicate materials. *Cement Concr Compos* 2011;33(2):163–70.
- [28] Das S, Yang P, Singh SS, Mertens JC, Xiao X, Chawla N, et al. Effective properties of a fly ash geopolymers: synergistic application of X-ray synchrotron tomography, nanoindentation, and homogenization models. *Cement Concr Res* 2015;78:252–62.
- [29] Lee H, Vimonsatit V, Chindaprasirt P. Mechanical and micromechanical properties of alkali activated fly-ash cement based on nano-indentation. *Construct Build Mater* 2016;107:95–102.
- [30] Ma Y, Ye G, Hu J. Micro-mechanical properties of alkali-activated fly ash evaluated by nanoindentation. *Construct Build Mater* 2017;147:407–16.
- [31] Lee H, Vimonsatit V, Chindaprasirt P, Ngo T, Mendis P. Creep properties of cement and alkali activated fly ash materials using nanoindentation technique. *Construct Build Mater* 2018;168:547–55.
- [32] Jennings HM, Thomas JJ, Gevenov JS, Constantinides G, Ulm F-J. A multi-technique investigation of the nanoporosity of cement paste. *Cement Concr Res* 2007;37(3):329–36.
- [33] De Jong MJ, Ulm F-J. The nanogranular behavior of CSH at elevated temperatures (up to 700 °C). *Cement Concr Res* 2007;37(1):1–12.
- [34] Vandamme M, Ulm F-J, Fonollosa P. Nanogranular packing of C-S-H at substoichiometric conditions. *Cement Concr Res* 2010;40(1):14–26.
- [35] Hu C, Gao Y, Zhang Y, Li Z. Statistical nanoindentation technique in application to hardened cement pastes: influences of material microstructure and analysis method. *Construct Build Mater* 2016;113:306–16.
- [36] Davydov D, Jirásek M, Kopecký L. Critical aspects of nano-indentation technique in application to hardened cement paste. *Cement Concr Res* 2011;41(1):20–9.
- [37] Hu C, Hou D, Li Z. Micro-mechanical properties of calcium sulfoaluminate cement and the correlation with microstructures. *Cement Concr Compos* 2017;80:10–6.
- [38] Hu C, Xu B, Ma H, Chen B, Li Z. Micromechanical investigation of magnesium oxychloride cement paste. *Construct Build Mater* 2016;105:496–502.
- [39] Chen JJ, Sorelli L, Vandamme M, Ulm FJ, Chanvillard G. A Coupled nanoindentation/SEM-EDS study on low water/cement ratio Portland cement paste: evidence for C-S-H/Ca (OH) 2 nanocomposites. *J Am Ceram Soc* 2010;93 (5):1484–93.
- [40] Provis JL, Lukey GC, van Deventer JS. Do geopolymers actually contain nanocrystalline zeolites? A reexamination of existing results. *Chem Mater* 2005;17 (12):3075–85.
- [41] Zhang Z, Wang H, Provis JL, Bullen F, Reid A, Zhu Y. Quantitative kinetic and structural analysis of geopolymers. Part 1. The activation of metakaolin with sodium hydroxide. *Thermochim Acta* 2012;539:23–33.
- [42] Zhang Z, Wang H, Yao X, Zhu Y. Effects of halloysite in kaolin on the formation and properties of geopolymers. *Cement Concr Compos* 2012;34(5):709–15.
- [43] Miller M, Bobko C, Vandamme M, Ulm F-J. Surface roughness criteria for cement paste nanoindentation. *Cement Concr Res* 2008;38(4):467–76.
- [44] Zhai C, Gan Y, Hanor D, Proust G, Retraint D. The role of surface structure in normal contact stiffness. *Exp Mech* 2016;56(3):359–68.
- [45] Lloyd RR, Provis JL, Smeaton KJ, van Deventer JS. Spatial distribution of pores in fly ash-based inorganic polymer gels visualised by Wood's metal intrusion. *Microporous Mesoporous Mater* 2009;126(1–2):32–9.
- [46] Bishop CM. Pattern recognition and machine learning. Springer; 2006.
- [47] Schwarz G. Estimating the dimension of a model. *Ann Stat* 1978;6(2):461–4.
- [48] Roa J, Jimenez-Pique E, Verge C, Tarrago J, Mateo A, Fair J, et al. Intrinsic hardness of constituent phases in WC-Co composites: nanoindentation testing, statistical analysis, WC crystal orientation effects and flow stress for the constrained metallic binder. *J Eur Ceram Soc* 2015;35(13):3419–25.
- [49] Ulm F-J, Vandamme M, Jennings HM, Vanzo J, Bentivegna M, Krakowiak KJ, et al. Does microstructure matter for statistical nanoindentation techniques? *Cement Concr Compos* 2010;32(1):92–9.
- [50] Constantinides G, Ulm F-J. The nanogranular nature of C-S-H. *J Mech Phys Solid* 2007;55(1):64–90.
- [51] Jennings HM. A model for the microstructure of calcium silicate hydrate in cement paste. *Cement Concr Res* 2000;30(1):101–16.
- [52] Duxson P, Provis JL, Lukey GC, Mallicoat SW, Kriven WM, Van Deventer JS. Understanding the relationship between geopolymers composition, microstructure and mechanical properties. *Colloids Surf, A* 2005;269(1–3):47–58.
- [53] De Vargas AS, Dal Molin DC, Vilela AC, Da Silva FJ, Pavão B, Veit H. The effects of Na₂O/SiO₂ molar ratio, curing temperature and age on compressive strength, morphology and microstructure of alkali-activated fly ash-based geopolymers. *Cement Concr Compos* 2011;33(6):653–60.
- [54] Singh GB, Subramanian KV. Influence of processing temperature on the reaction product and strength gain in alkali-activated fly ash. *Cement Concr Compos* 2019; 95:10–8.
- [55] Sun Z, Vollpracht A. One year geopolymersation of sodium silicate activated fly ash and metakaolin geopolymers. *Cement Concr Compos* 2019;95:98–110.
- [56] Constantinides G, Ulm F-J. The effect of two types of CSH on the elasticity of cement-based materials: results from nanoindentation and micromechanical modeling. *Cement Concr Res* 2004;34(1):67–80.
- [57] Pelisser F, Gleize PJP, Mikowski A. Effect of the Ca/Si molar ratio on the micro/nanomechanical properties of synthetic CSH measured by nanoindentation. *J Phys Chem* 2012;116(32):17219–27.